Gobbo, P., Patil, A. J., Li, M., Harniman, R., Briscoe, W. H., & Mann, S. (2018). Programmed assembly of synthetic protocells into thermoresponsive prototissues. *Nature Materials*, *17*(12), 1145-1153. https://doi.org/10.1038/s41563-018-0183-5

Peer reviewed version

Programmed assembly of synthetic protocells into thermoresponsive prototissues

Pierangelo Gobbo, Avinash J. Patil, Mei Li, Robert Harniman, Wuge H. Briscoe and Stephen Mann*

Centre for Protolife Research and Centre for Organized Matter Chemistry, School of Chemistry, University of Bristol, Bristol, BS8 1TS (UK). E-mail: s.mann@bristol.ac.uk

Although several new types of synthetic cell-like entities, i.e. protocells, are now available, their structural integration into spatially interlinked prototissues that communicate and display coordinated functions remains a considerable challenge. Here we describe the programmed assembly of synthetic prototissue constructs based on the bio-orthogonal adhesion of a spatially confined binary community of protein-polymer protocells, termed proteinosomes. The thermoresponsive properties of the interlinked proteinosomes are used collectively to generate prototissue spheroids capable of reversible contractions that can be enzymatically modulated and exploited for mechanochemical transduction. Overall, our methodology opens up a route to the fabrication of artificial tissue-like materials capable of collective behaviours, and addresses important emerging challenges in bottom-up synthetic biology and bioinspired engineering.

Living tissues and organs comprise spatially interlinked consortia of specialized cells that communicate and display collective behaviours within an integrated three-dimensional (3D) environment. Mimicking these complex living ensembles through the design and construction of artificial tissue-like systems (prototissues) based on the controlled assembly and functional integration of synthetic cell-like entities (protocells) is a major challenge that has important technological implications in bottom-up synthetic biology, bioinspired tissue engineering and microscale engineering of soft machines and devices [1]. Recently, a range of different synthetic protocells based on lipid vesicles [2-5], polymersomes [6-9], polypeptide capsules [10,11], dendrimersomes [12,13], inorganic colloidosomes [14-17], coacervate micro-droplets [18-22] and semi-permeable protein-polymer microcapsules (proteinosomes) [23-27] have been reported. However, the development of synthetic prototissues based on assembly of these protocells into higher-order spatial micro-architectures such as spheroidal clusters and sheet-like aggregates that exhibit collective functions due to their structural integration remains a considerable challenge. To date, extended unstructured amorphous aggregates of polymerosomes have been assembled in water by uncontrolled interfacial chemical reactivity [28-31], and clusters of limited numbers of lipid-stabilized water-in-oil emulsion droplets produced by microfluidic fabrication [32-41] or droplet adhesion [35-41]. In a series of breakthrough studies, Bayley and colleagues have demonstrated the use of 3D printing to spatially organize large numbers of lipid-coated water-in-oil droplets in the form of a rudimentary prototissue capable of membrane protein-mediated electrical communication, macroscopic deformation, and light-induced gene expression [42,43].

In this paper, we describe the programmed assembly of spatially integrated prototissue spheroids that comprise a binary community of bio-orthogonally linked proteinosome-based protocells capable of thermoresponsive collective behaviours such as enzymatically modulated reversible contraction, and mechanochemical transduction. These behaviours are based on coordinated interactions between multiple chemically coupled proteinosomes assembled at equilibrium and are therefore considered to be collective in the general sense rather than as a consequence of non-equilibrium (active) behaviour. For this, we synthesize two new types of thermally responsive protein-polymer nanoconjugates with either pendent azide or strained alkyne functionalities, and use the amphiphilic conjugates to prepare two separate populations of bio-orthogonally reactive proteinosomes. Mixed populations of the proteinosomes are spatially confined using a water-in-oil-in-water (w/o/w) Pickering emulsion procedure and then structurally linked *in situ* via an interfacial strain-promoted alkyne-azide cycloaddition (I-SPAAC) reaction [44-46] to afford synthetic tissue-like spheroids upon removal of the oil phase. Significantly, individual spheroids exhibit reversible changes in volume due to collective contraction/relaxation of the ligated proteinosomes when transitioned above and below the lower critical solution temperature (LCST) of the thermoresponsive polymer. We show that the contraction/relaxation cycles can be sustained reversibly for tens of cycles at constant frequency and amplitude, and that the process can be switched off during the temperature cycling by internalized enzyme-mediated hydrogelation. Finally, we demonstrate a rudimentary form of prototissue mechanochemical transduction by coupling the reversible contraction/relaxation behaviour of the spheroids to the down/up regulation of a coordinated enzyme cascade housed specifically within the bio-orthogonally linked proteinosomes.

Programmed assembly of synthetic protocells into prototissues

Cationized bovine serum albumin (BSA) was covalently conjugated to poly(*N*-isopropylacrylamide-co-methacrylic acid) (PNIPAM-co-MAA) and the nanoconjugates functionalized with at least 78 azide (N_3) or 59 strained alkyne (bicyclo[6.1.0]nonyne (BCN)) functional groups capable of undergoing an I-SPAAC reaction (Figure 1a,b, Supplementary Figures 1-11, and Methods). Both bio-orthogonal nanoconjugates exhibited a reversible temperature-dependent change in hydrodynamic diameter between 35 and 45 °C (LCST = *ca*. 37 °C; Supplementary Figure 12, 13), and were bio-orthogonally reactive when mixed in aqueous solution at room temperature for 15 h (Supplementary Figure 14, 15). Given the potential for bio-orthogonal chemistry between the nanoconjugates, we anticipated that sustained contact in water between cross-linked proteinosomes prepared with either an N_3- or BCN-functionalized membrane would lead to similar SPAAC interactions at the microscale level to produce closely packed, covalently linked protocell consortia with spatially interlinked tissue-like structures. We achieved this using a stepwise process based on the encapsulation of 1:1 binary populations of the bio-orthogonal proteinosomes (mean diameter, *ca.* 30 μm; volume, 10 ± 3 pL) within w/o/w Pickering emulsion droplets stabilized by a non-bio-orthogonal membrane of BSA/PNIPAM-co-MAA nanoconjugates that was stabilized by a crosslinker containing a disulphide bond (NHS-PEG16-DS) (Figure 1c-e). Fluorescence microscopy images of the emulsion droplets showed a nested arrangement of water-filled bio-

orthogonally reactive proteinosomes that were closely packed, dispersed in an encapsulated oil phase, and housed within a bio-orthogonally non-reactive host proteinosome (Figure 1f and Supplementary Figure 16). Significantly, removal of the encapsulated oil triggered bio-orthogonal ligation of the guest proteinosomes to produce membrane-bounded spheroids (mean size, *ca.* 70 μm; volume, 180 ± 80 pL) with a spatially integrated tissue-like structure (Figure 1g and Supplementary Figure 17 and Supplementary Video 1).

The above observations indicated that high levels of bio-orthogonal adhesion over relatively short periods of time (typically within 6-8 h) could be achieved by spatial confinement of the reactive proteinosomes at high packing densities. Cross-linking of the outer non-bio-orthogonal BSA/PNIPAM-co-MAA membrane with NHS-PEG16-DS was critical to prevent disassembly of the caged spheroids prior to completion of the bio-orthogonal adhesion process (Supplementary Figure 18). Moreover, to confirm that the internalized proteinosome network was bio-orthogonally ligated, we chemically disassembled the outer membrane to produce uncaged spheroids that exhibited no change in size (*ca.* 70 μm; volume, 180 ± 80 pL), shape or structural integrity in water (Figure 1h, Supplementary Figure 19 and Supplementary Video 2). The results indicated that the number of bio-orthogonal chemistry membrane-mediated adhesions formed at the contact interface between adjacent proteinosomes was sufficient to generate a self-supporting prototissue. In contrast, caged assemblies of non-bio-orthogonal crosslinked proteinosomes became dispersed after chemical disassembly of the outer membrane (Supplementary Figure 20).

The internal structure of the tissue-like spheroids was investigated using fluorescence microscopy to determine the protocell neighbour number (PNN) (Supplementary Figure 21). For a 1:1 binary population of bio-orthogonal proteinosomes, the average PNN was 4 with each protocell in contact with two proteinosomes of the same kind and with two proteinosomes carrying the complementary bio-orthogonal group. Increasing the number ratio between the strained alkyne- and azide-functionalized proteinosomes to 5:1 and 10:1 did not change the average PNN. Under these conditions, most of the protocells were surrounded by BCN-functionalized proteinosomes. In each case, we attributed the low PNN to the relatively high numbers of proteinosomes located at the surface of the spheroids compared with those positioned within the interior of the prototissue clusters.

The above procedures were highly reproducible and could be adapted to increase the size of the tissue-like spheroids and number of bio-orthogonally linked constituent proteinosomes by decreasing the concentration of the non-bio-orthogonal BSA/PNIPAM-co-MAA nanoconjugates (Supplementary Figure 22, 23 and Supplementary Table 1). Typically, caged/uncaged spheroids with average volumes ranging from approximately 180 to 900 pL (mean sizes, 70 and 120 μm, respectively) and consisting of a total number (*n*) of 20 to 90 interlinked proteinosomes could be prepared. These observations were consistent with previous studies[23], which showed that decreases in the concentration of the protein-polymer nanoconjugates produced larger proteinosomes.

Reversible contractions in thermoresponsive prototissue spheroids

Having established that an I-SPAAC reaction could be successfully employed to produce integrated synthetic cell-like masses of caged or uncaged proteinosomes, we investigated whether the thermoresponsive properties associated with the crosslinked BSA/PNIPAM nanoconjugate membrane [23] could be exploited collectively to generate synthetic prototissues capable of sustained contractions (Figure 2a). To achieve this, we heated aqueous dispersions containing uncaged tissue-like clusters (*n* = 10-30) above the LCST of PNIPAM-co-MAA and monitored the temperature-dependent changes in the equilibrium size of the prototissues by fluorescence microscopy. Remarkably, individual spheroids underwent shrinking of up to 37 ± 5 vol% at 47 °C (Figure 2b). Onset of the volume contraction occurred at *ca*. 37 °C and progressed approximately linearly up to 47 °C. Corresponding experiments with caged prototissue spheroids revealed similar temperature-dependent changes in contractibility (Supplementary Figure 24), indicating that the collective thermoresponsive behaviour was not dependent on the presence of a non-bio-orthogonally linked outer membrane. In contrast, a volume contraction of only 11 ± 2 vol% was determined at 47 °C for caged assemblies comprising a binary population of closely packed non-bio-orthogonally linked BSA/PNIPAM-co-MAA proteinosomes (Supplementary Figure 25). Under these conditions the contractile response was analogous to that observed for freely dispersed individual proteinosomes, which showed a membrane transition temperature of *ca.* 37 °C associated with shrinking of up to only 10 ± 1 vol% at 47 °C (Figure 2b). Significantly, decreasing the temperature from 47 to below 35 °C resulted in expansion of the prototissue and relaxation back to the original size and morphology (Figure 2b).

The above results indicate that bio-orthogonal adhesion of the constituent proteinosomes was primarily responsible for the collective deswelling of the prototissue spheroids. This proposal was also consistent with measurements of the contractile properties associated with caged or uncaged prototissue spheroids comprising different numbers (*n*) of constituent proteinosomes (Figure 2c). Increasing *n* from values of 5 to 170 was associated with a non-linear increase in the percentage volume contraction from 30 vol% to a limiting threshold of *ca*. 45 vol%, and was independent of whether the prototissue spheroids were enclosed or not in an outer membrane. We attributed the progressive increase in contractibility to a concomitant increase in the number of coupled bio-orthogonal interactions that enabled the void space in the core of the spheroids to be diminished more effectively until the limiting threshold was reached.

Prototissue spheroids exhibited reversible contraction/relaxation behaviour as the temperature was cycled slowly through the LCST of PNIPAM-co-MAA. Typically, each equilibrium cycle required *ca.* 10 min. We increased the rate of oscillation under kinetic conditions by heating the surrounding aqueous solution to 45 °C using a nichrome wire connected to a DC power generator, followed by use of a water/ice/NaCl bath to lower the temperature back to 35 °C. As a consequence, we were able to produce prototissue spheroids that exhibited collective contractions that could be sustained reversibly at a constant amplitude for at least ten cycles at frequencies of 2.5 oscillations min^{-1} (Figure 2d). The spheroids retained their original volume after each contraction/relaxation cycle, and in general, contracted and relaxed homogeneously and symmetrically during the thermal cycles (Supplementary

Video 3). However, buckling of the bio-orthogonally linked constituent proteinosomes was observed in some of the spheroids (Supplementary Video 4), possibly due to the size heterogeneity of the constituent proteinosomes.

Given the reversibility of the contraction/relaxation cycles, we determined the expansion force associated with the thermoresponsive behavior of individual prototissue spheroids using atomic force microscopy (AFM). An individual spheroid was heated to 50 °C, and the contracted assemblage then trapped between a mica substrate and AFM cantilever (Figure 2e and Supplementary Figure 26). Upon cooling, a rapid increase in the induced radial force up to a value of 62.2 ± 6.5 nN was observed as the prototissue spheroid expanded back to its native state below the LCST (Figure 2f). The prototissue spheroid is structurally analogous to a closed-cell foam[47], although explicit analytic expressions to account for the elastic properties of such a micro-foam with spatially confined cells partitioned by highly permeable nanometer-thick membranes are not currently available. We considered the elastic property of each spheroid to be dominated by elastic bending and stretching of the membranes of the constituent proteinosomes, and assumed that the viscous drag and the incompressibility of water upon prototissue volume change were negligible (Supplementary Notes, section 2.2). We estimated the Young's moduli (E_s) of the relaxed and contracted crosslinked proteinosome membrane as 2.0 kPa and 9.3 kPa, respectively, using the de Gennes scaling term, $E_s \sim k_B T/\xi^3$, where $k_B T = 4.11\times10^{-21}$ J at 298 K, and ξ is the membrane mesh size (or correlation length). The latter was estimated from $\xi \sim 2R_s$ for a Stokes radius R_s derived from the molecular weight cut-off determined from studies of the membrane permeability of FITC-dextran (Figure 4a-c). Using the Hertzian theory of contact mechanics and the above E_s values, we calculated a lower limit of the force exerted on the AFM cantilever as 4 – 18 nN. This was comparable with the experimentally detected force of 62.2 nN, suggesting that the theoretical model was consistent with the observed thermoresponsive behaviour of the prototissue spheroids. Interestingly, the force exerted by the prototissue spheroid was commensurate with typical forces determined for collective behavior in biological systems such beating cardiomyocyte clusters[48], migrating endothelial cells[49], and motile bacteria colonies[50], all of which fall within the range of 1 – 100 nN.

Enzyme-mediated modulation of prototissue contractibility

Although the reversible contraction frequency was determined by external control of the temperature ramp, we sought to internally switch off or modulate the amplitude of the collective behaviour by a process involving the coordinated enzyme-mediated supramolecular assembly of a peptide hydrogel specifically within the prototissue spheroids (Figure 3a and Supplementary Figure 27, 28). In the presence of the peptide (N-[(9H-fluoren-9-ylmethoxy)carbonyl]-L-alanyl-L-alanine; Fmoc-Ala-Ala-OH) and in the absence of substrate (maltose) at pH 8.5, reversible oscillatory contractions were observed between 25 and 47 °C for spheroids comprising a 1:1 mixture of bio-orthogonally linked α-glucosidase (AGL)-containing N_3-BSA/PNIPAM-co-MAA and glucose oxidase (GOx)-containing BCN-BSA/PNIPAM-co-MAA proteinosomes (Figure 3b,c and Supplementary Figure 29). In contrast, addition of maltose and

subsequent hydrogelation of the tissue-like spheroids resulted in progressive dampening of the amplitude and switching off of the temperature-induced reversible contractions (Figure 3b,c and Supplementary Figure 30). Although a normal contraction of *ca.* 40 vol% was determined for the first heating step from 25 and 47 °C, subsequent cooling did not reinstate the native state but resulted in arrested relaxation to produce spheroids that remained partially constricted with volume contractions of *ca.* 25 %. Subsequent heating/cooling cycles showed that relaxation of the individual spheroids decreased in amplitude after each temperature cycle until the reversible contractibility was eliminated after the fifth cycle to produce a thermally non-responsive prototissue with a constant volume contraction of *ca.* 40% (Figure 3b,c). Interestingly, restoration of the maximum amplitude and reversible contractibility between 25 and 47 °C was achieved by removing excess maltose and peptide, and raising the pH to 8.5, which disassembled the hydrogel within the spheroids (Figure 3b,c). The reversibility could then be switched off again by re-instating the enzyme-mediated re-formation of the peptide hydrogel.

These observations confirmed that curtailment of the spheroid relaxation was dependent on the presence of the peptide hydrogel. Although the precise mechanism responsible for the onset of irreversibility was not elucidated in detail, differential scanning calorimetry measurements indicated that the peptide hydrogel was thermally stable at the temperatures used to study amplitude modulations in the contractile prototissue (Supplementary Figure 31). In addition, lowering the maximum temperature in the thermal cycles from 47 to 40 °C eliminated the irreversible contractibility to produce hydrogelated spheroids capable of undergoing oscillatory transitions exhibiting a constant but reduced amplitude of *ca*. 20 vol% (Supplementary Figure 32). These observations suggested that progressive inhibition in the relaxation of the hydrogelated spheroids was associated with stabilization of high levels of wrinkling of the bio-orthogonally linked proteinosome membranes. One possibility is that localized reconstruction of the peptide nanofilaments around the PNIPAM-co-MAA copolymer chains of the membrane building blocks results in immobilization of the contracted spheroids due to steric hindrance at the molecular level.

Mechanochemical transduction within prototissue spheroids

Given the thermoresponsive behaviour of the bio-orthogonally linked proteinosome spheroids we investigated whether the collective contractile properties could be used to influence the ability of the synthetic prototissues to sense the surrounding chemical environment and perform cooperative internalized enzyme catalysis within proteinosome volumes of *ca.* 10 pL. As a step towards this goal, we first investigated whether the collective contractile properties could influence the permeability of the prototissue spheroid. To do this, we incubated the spheroids at 25 or 47 °C in the presence of a series of FITC-labelled dextrans with different molecular weights ranging from 4 to 150 kDa (Figure 4 a,b), and measured the diffusion of the macromolecules into the prototissue spheroids using optical and fluorescence microscopy. The results indicated that the MWCO associated with the prototissue spheroid was *ca.* 80 kDa at 25 °C and 30 kDa at 47 °C, (Figure 4c). The drastic reduction of *ca*. 50 kDa accompanying the transition from the relaxed to the contracted form was also obtained for caged

prototissue spheroids. In contrast, analogous experiments using either strained alkyne- or azide-functionalized single proteinosomes showed a MWCO of *ca.* 100 kDa, which within experimental error was temperature-independent (Supplementary Figure 33). We attributed these differences to the collective mechanical properties of the prototissue spheroids originating from the chemical ligation and spatial integration of the individual proteinosomes into the interlinked assemblages of protocells.

Inspired by the above observations, and as a step towards a rudimentary form of synchronized mechanochemical transduction, we prepared uncaged prototissues (*n* = 10-30) from a binary population of FITC-labelled BCN-BSA/PNIPAM-co-MAA and unlabelled N_3-BSA/PNIPAM-co-MAA proteinosomes that were pre-loaded with entrapped GOx or horseradish peroxidase (HRP), respectively. We then perfused the synthetic prototissues in an aqueous solution containing proteinosome-permeable molecular substrates (glucose/Amplex Red or glucose/ABTS) to initiate a spatially coupled GOx/HRP enzyme cascade reaction within expanded or contracted bio-orthogonally linked spheroids (Figure 4d). Initially, we used fluorescence microscopy to determine the location of the GOx-containing FITC-labelled BCN-BSA/PNIPAM-co-MAA proteinosomes within individual prototissue spheroids, and to monitor the onset and *in situ* development of the entrapped enzyme cascade when the spheroids were incubated at 25 °C with a mixture of glucose and Amplex Red (Figure 4e,f and Supplementary Video 5). Typically, the onset of red fluorescence due to initial production of resorufin in the HRP-containing N_3-BSA/PNIPAM-co-MAA proteinosomes occurred within 50 s, followed by leakage into the neighbouring GOx-containing proteinosomes and external environment. In contrast, control experiments involving uncaged spheroids lacking either GOx or HRP showed no increases in fluorescence (Supplementary Figure 34) due to the inability of these prototissues to sense glucose in the surrounding environment or synthesize resorufin, respectively.

Having established that molecular substrates can diffusion freely at room temperature into the bio-orthogonally linked matrix of the uncaged prototissue spheroids to access the proteinosome-encapsulated enzymes via passive membrane uptake, we explored the possibility of coupling the temperature-dependent collective contractile properties to the sensing and coordinated catalytic properties of the synthetic tissue-like assemblies. If feasible, such a strategy could provide a step towards a synthetic cell-like tissue exhibiting a rudimentary form of synchronized mechanochemical transduction. As a proof-of-concept, we monitored the initial rate of reaction for the prototissue-confined GOx/HRP cascade in the presence of glucose and ABTS at a range of temperatures between 25 and 45 °C (Figure 4g). Interestingly, whereas increases in the initial reaction rate were observed between 25 and 45 °C for GOx/HRP in free solution or for a dispersed binary population of GOx-containing and HRP-containing proteinosomes, the collective contractile behaviour of the prototissue spheroids gave rise to an approximate 53% decrease in the initial reaction rate over the same temperature range. Initially, an increase in the reaction rate was observed when the temperature was raised to 30 °C, but this was followed by progressive decreases in enzyme activity at higher temperatures. Reducing the temperature from 45 to 25 °C indicated that the contractile-dependent changes in enzyme activity were reversible (Figure 4g).

Outlook

As a step towards the programmed assembly of synthetic protocells into tissue-like constructs, we use bio-orthogonal chemistry to engineer the membrane reactivity of a spatially confined binary population of proteinosomes. Bio-orthogonal adhesion of the densely packed proteinosomes produces membrane-caged or uncaged prototissue spheroids that are typically 40-100 μm in size and consist of 10-30 semi-permeable protein-polymer microcapsules. The prototissue spheroids are capable of housing proteinosome-encapsulated enzyme cascade reactions, and show enhanced volume contractions compared with caged assemblies of unbound non-bio-orthogonal proteinosomes or individual proteinosomes when heated above 35 °C. We exploit the collective contractibility to produce tissue-like constructs capable of reversible and sustainable contractions that can be enzymatically modulated and exploited for the mechanochemical transduction of a proteinosome-coordinated enzyme cascade. The emergence of the higher-order behaviour arises from collective interactions and coordinated responses that are facilitated by spatial integration of the synthetic protocells within the prototissue spheroids.

From a more general perspective, due to the covalent nature of the inter-proteinosome junctions, the spheroids display high stability in water (> 6 months) thereby opening up possibilities for building enzymatically active tissue-like structures capable of internalized protocell-protocell communication and sensing of chemical stimuli in the surrounding environment. Significantly, proteinosome-based protocell models exhibiting gene-directed protein synthesis, membrane-gated enzyme activity, selective membrane permeability, membrane-mediated tandem catalysis, protease-mediated disassembly, and hierarchical storage and release behaviour have been recently demonstrated [22-26], suggesting that it should be possible to fabricate synthetic prototissues with a wide range of collective functions and behaviours. Our methodology therefore opens up a route from the synthetic construction of individual protocell models to the co-assembly and spatial integration of multi-protocellular structures that combine the specialization of individual protocell types with collective properties of the ensemble. In general, the rational design and fabrication of prototissues bridges an important gap in bottom-up synthetic biology strategies, and contributes to the development of new bioinspired materials for potential use in areas such as tissue engineering, cell-protocell interactions (drug delivery, signalling, gene regulation) and micro-bioreactor technology.

References

1 Mantri, S. & Sapra, K. T. Evolving protocells to prototissues: rational design of a missing link. *Biochem. Soc. Trans.* **41**, 1159-1165, doi:10.1042/BST20130135 (2013).

2 Lentini, R. *et al.* Two-Way Chemical Communication between Artificial and Natural Cells. *ACS Cent. Sci.* **3**, 117-123, doi:10.1021/acscentsci.6b00330 (2017).

3 Qiao, H. *et al.* Encapsulation of Nucleic Acids into Giant Unilamellar Vesicles by Freeze-Thaw: a Way Protocells May Form. *Orig. Life Evol. Biosph.*, doi:10.1007/s11084-016-9527-9 (2016).

4 Altamura, E. *et al.* Highly oriented photosynthetic reaction centers generate a proton gradient in synthetic protocells. *Proc. Natl. Acad. Sci. U. S. A.* **114**, 3837-3842, doi:10.1073/pnas.1617593114 (2017).

5 Adamala, K. P., Engelhart, A. E. & Szostak, J. W. Collaboration between primitive cell membranes and soluble catalysts. *Nat. Commun.* **7**, 11041, doi:10.1038/ncomms11041 (2016).

6 Jang, W. S. *et al.* Enzymatically triggered rupture of polymersomes. *Soft Matter* **12**, 1014-1020, doi:10.1039/c5sm01881a (2016).

7 Peyret, A. *et al.* Polymersome Popping by Light-Induced Osmotic Shock under Temporal, Spatial, and Spectral Control. *Angew. Chem. Int. Ed.* **56**, 1566-1570, doi:10.1002/anie.201609231 (2017).

8 Schmitt, C., Lippert, A. H., Bonakdar, N., Sandoghdar, V. & Voll, L. M. Compartmentalization and Transport in Synthetic Vesicles. *Front. Bioeng. Biotechnol.* **4**, 19, doi:10.3389/fbioe.2016.00019 (2016).

9 Che, H. & Hest, J. C. M. v. Stimuli-responsive polymersomes and nanoreactors. *J. Mater. Chem. B*, 4632-4647, doi:10.1039/C6TB01163B (2016).

10 Bellomo, E. G., Wyrsta, M. D., Pakstis, L., Pochan, D. J. & Deming, T. J. Stimuli-responsive polypeptide vesicles by conformation-specific assembly. *Nat. Mater.* **3**, 244-248, doi:10.1038/nmat1093 (2004).

11 Holowka, E. P., Sun, V. Z., Kamei, D. T. & Deming, T. J. Polyarginine segments in block copolypeptides drive both vesicular assembly and intracellular delivery. *Nat. Mater.* **6**, 52-57, doi:10.1038/nmat1794 (2007).

12 Xiao, Q. *et al.* Bioactive cell-like hybrids coassembled from (glyco)dendrimersomes with bacterial membranes. *Proc. Natl. Acad. Sci. U. S. A.* **113**, E1134-1141, doi:10.1073/pnas.1525589113 (2016).

13 Percec, V. *et al.* Self-assembly of Janus dendrimers into uniform dendrimersomes and other complex architectures. *Science* **328**, 1009-1014, doi:10.1126/science.1185547 (2010).

14 Akkarachaneeyakorn, K., Li, M., Davis, S. A. & Mann, S. Secretion and Reversible Assembly of Extracellular-like Matrix by Enzyme-Active Colloidosome-Based Protocells. *Langmuir* **32**, 2912-2919, doi:10.1021/acs.langmuir.6b00553 (2016).

15 Sun, S. *et al.* Chemical Signaling and Functional Activation in Colloidosome-Based Protocells. *Small* **12**, 1920-1927, doi:10.1002/smll.201600243 (2016).

16 Li, M., Huang, X. & Mann, S. Spontaneous growth and division in self-reproducing inorganic colloidosomes. *Small* **10**, 3291-3298, doi:10.1002/smll.201400639 (2014).

17 Li, M., Harbron, R. L., Weaver, J. V., Binks, B. P. & Mann, S. Electrostatically gated membrane permeability in inorganic protocells. *Nat. Chem.* **5**, 529-536, doi:10.1038/nchem.1644 (2013).

18 Yin, Y. *et al.* Non-equilibrium behaviour in coacervate-based protocells under electric-field-induced excitation. *Nat. Commun.* **7**, 10658, doi:10.1038/ncomms10658 (2016).

19 Williams, D. S., Patil, A. J. & Mann, S. Spontaneous structuration in coacervate-based protocells by polyoxometalate-mediated membrane assembly. *Small* **10**, 1830-1840, doi:10.1002/smll.201303654 (2014).

20 Dora Tang, T. Y. *et al.* Fatty acid membrane assembly on coacervate microdroplets as a step towards a hybrid protocell model. *Nat. Chem.* **6**, 527-533, doi:10.1038/nchem.1921 (2014).

21 Dora Tang, T. Y., van Swaay, D., deMello, A., Ross Anderson, J. L. & Mann, S. In vitro gene expression within membrane-free coacervate protocells. *Chem. Commun.* **51**, 11429-11432, doi:10.1039/c5cc04220h (2015).

22 Qiao, Y., Li, M., Booth, R. & Mann, S. Predatory behaviour in synthetic protocell communities. *Nat. Chem.* **9**, 110-119, doi:10.1038/nchem.2617 (2017).

23 Huang, X. *et al.* Interfacial assembly of protein-polymer nano-conjugates into stimulus-responsive biomimetic protocells. *Nat. Commun.* **4**, 2239, doi:10.1038/ncomms3239 (2013).

24 Huang, X., Li, M. & Mann, S. Membrane-mediated cascade reactions by enzyme-polymer proteinosomes. *Chem. Commun.* **50**, 6278-6280, doi:10.1039/c4cc02256d (2014).

25 Huang, X., Patil, A. J., Li, M. & Mann, S. Design and construction of higher-order structure and function in proteinosome-based protocells. *J. Am. Chem. Soc.* **136**, 9225-9234, doi:10.1021/ja504213m (2014).

26 Liu, X. *et al.* Hierarchical Proteinosomes for Programmed Release of Multiple Components. *Angew. Chem. Int. Ed.* **55**, 7095-7100, doi:10.1002/anie.201601427 (2016).

27 Wen, P. *et al.* Coordinated Membrane Fusion of Proteinosomes by Contact-Induced Hydrogel Self-Healing. *Small*, doi:10.1002/smll.201700467 (2017).
28 Jin, H. *et al.* Reversible and large-scale cytomimetic vesicle aggregation: light-responsive host-guest interactions. *Angew. Chem. Int. Ed.* **50**, 10352-10356, doi:10.1002/anie.201103164 (2011).
29 Jin, H. *et al.* Cytomimetic large-scale vesicle aggregation and fusion based on host-guest interaction. *Langmuir* **28**, 2066-2072, doi:10.1021/la203857s (2012).
30 Jin, H., Huang, W., Zheng, Y., Zhou, Y. & Yan, D. Construction of macroscopic cytomimetic vesicle aggregates based on click chemistry: controllable vesicle fusion and phase separation. *Chemistry* **18**, 8641-8646, doi:10.1002/chem.201201401 (2012).
31 Jin, H. *et al.* Three-component vesicle aggregation driven by adhesion interactions between Au nanoparticles and polydopamine-coated nanotubes. *Chem. Commun.* **50**, 6157-6160, doi:10.1039/c4cc00609g (2014).
32 Bai, Y. *et al.* A double droplet trap system for studying mass transport across a droplet-droplet interface. *Lab Chip* **10**, 1281-1285, doi:10.1039/b925133b (2010).
33 Zagnoni, M. & Cooper, J. M. A microdroplet-based shift register. *Lab Chip* **10**, 3069-3073, doi:10.1039/c0lc00219d (2010).
34 Stanley, C. E. *et al.* A microfluidic approach for high-throughput droplet interface bilayer (DIB) formation. *Chem. Commun.* **46**, 1620-1622, doi:10.1039/b924897h (2010).
35 Elani, Y., Law, R. V. & Ces, O. Vesicle-based artificial cells as chemical microreactors with spatially segregated reaction pathways. *Nat. Commun.* **5**, 5305, doi:10.1038/ncomms6305 (2014).
36 Dixit, S. S., Kim, H., Vasilyev, A., Eid, A. & Faris, G. W. Light-driven formation and rupture of droplet bilayers. *Langmuir* **26**, 6193-6200, doi:10.1021/la1010067 (2010).
37 Holden, M. A., Needham, D. & Bayley, H. Functional bionetworks from nanoliter water droplets. *J. Am. Chem. Soc.* **129**, 8650-8655, doi:10.1021/ja072292a (2007).
38 Leptihn, S. *et al.* Constructing droplet interface bilayers from the contact of aqueous droplets in oil. *Nat. Protoc.* **8**, 1048-1057, doi:10.1038/nprot.2013.061 (2013).
39 Hwang, W. L., Chen, M., Cronin, B., Holden, M. A. & Bayley, H. Asymmetric droplet interface bilayers. *J. Am. Chem. Soc.* **130**, 5878-5879, doi:10.1021/ja802089s (2008).
40 Milianta, P. J., Muzzio, M., Denver, J., Cawley, G. & Lee, S. Water Permeability across Symmetric and Asymmetric Droplet Interface Bilayers: Interaction of Cholesterol Sulfate with DPhPC. *Langmuir* **31**, 12187-12196, doi:10.1021/acs.langmuir.5b02748 (2015).
41 Villar, G., Heron, A. J. & Bayley, H. Formation of droplet networks that function in aqueous environments. *Nat. Nanotechnol.* **6**, 803-808, doi:10.1038/nnano.2011.183 (2011).
42 Booth, M. J., Schild, V. R., Graham, A. D., Olof, S. N. & Bayley, H. Light-activated communication in synthetic tissues. *Sci. Adv.* **2**, e1600056, doi:10.1126/sciadv.1600056 (2016).
43 Villar, G., Graham, A. D. & Bayley, H. A tissue-like printed material. *Science* **340**, 48-52, doi:10.1126/science.1229495 (2013).
44 Gobbo, P., Novoa, S., Biesinger, M. C. & Workentin, M. S. Interfacial strain-promoted alkyne-azide cycloaddition (I-SPAAC) for the synthesis of nanomaterial hybrids. *Chem. Commun.* **49**, 3982-3984, doi:10.1039/c3cc41634h (2013).
45 Gobbo, P. *et al.* Versatile strained alkyne modified water-soluble AuNPs for interfacial strain promoted azide-alkyne cycloaddition (I-SPAAC). *J. Mater. Chem. B* **2**, 1764-1769, doi:10.1039/c3tb21799j (2014).
46 Luo, W. *et al.* "Shine & Click" Photo-Induced Interfacial Unmasking of Strained Alkynes on Small Water-Soluble Gold Nanoparticles. *Chemistry* **23**, 1052-1059, doi:10.1002/chem.201603398 (2017).
47 Gibson, L. J. & Ashby, M. F. Cellular solids - Structure and Properties. *Cambridge University Press* (2014).
48 Liu, J., Sun, N., Bruce, M. A., Wu, J. C. & Butte, M. J. Atomic force mechanobiology of pluripotent stem cell-derived cardiomyocytes. *PLoS One* **7**, e37559, doi:10.1371/journal.pone.0037559 (2012).
49 du Roure, O. *et al.* Force mapping in epithelial cell migration. *Proc. Natl. Acad. Sci. U. S. A.* **102**, 2390-2395, doi:10.1073/pnas.0408482102 (2005).
50 Sabass, B., Koch, M. D., Liu, G., Stone, H. A. & Shaevitz, J. W. Force generation by groups of migrating bacteria. *Proc. Natl. Acad. Sci. U. S. A.* **114**, 7266-7271, doi:10.1073/pnas.1621469114 (2017).

Methods

1. Materials

All reagents were used as received unless otherwise stated. *N*-isopropylacrylamide, methacrylic acid (MAA), azobisisobutyronitrile (AIBN), diethyl ether (Et_2O), bovine serum albumin (BSA), fluorescein isothiocyanate (FITC), rhodamine isothiocyanate (RITC), hexamethylenediamine, *N*-[(1*R*,8*S*,9*s*)-bicyclo[6.1.0]non-4-yn-9-ylmethyloxycarbonyl]-1,8-diamino-3,6-dioxaoctane (BCN-NH_2), 11-azido-3,6,9-trioxaundecan-1-amine (N_3-NH_2), bis-*N*-succinimidyl polyethylene glycol (NHS-PEG35), deuterated chloroform ($CDCl_3$) (99.8 atom %), 4,7,10,13,16,19,22,25,32,35,38,41,44,47,50,53-hexadecaoxa-28,29-dithiahexapentacontanedioic acid di-*N*-succinimidyl ester (NHS-PEG16-DS)**,** 2-ethyl-1-hexanol**,** glutathione (GSH), dithiothreitol (DTT), dihydroxyacetophenone (DHAP), diammonium hydrogen citrate (DAHC), trifluoroacetic acid (TFA), glucose oxidase (GOx) (252100 U/mg), horseradish peroxidase (HRP) (172.2 U/mg), α-glucosidase (ALG,19.3 U/mg) and maltose were purchased from Sigma-Adrich. Acetonitrile, Amplex Red, DyLight 405 and Hoechst 33258 were purchased from Thermo Fisher Scientific. Hexanes and glucose was purchased from VWR. *N*-ethyl-*N'*-(3-dimethylaminopropyl) carbodiimide hydrochloride (EDAC) from Alfa Aesar, and N-[(9H-fluoren-9-ylmethoxy)carbonyl]-L-alanyl-L-alanine (Fmoc-Ala-Ala-OH) was purchased from Bachem. Dialysis bags with MWCO 1,000 or 12,000-14,000 Da were purchased from Millipore.

2. Preparation of synthetic tissue-like spheroids

Alkyne- and azide-functionalized proteinosomes in 2-ethly-1-hexanol (oil) were prepared in two separate 1.75 mL screw-cap vials. To prepare the alkyne-functionalized proteinosomes, 30 μL of an aqueous solution (8 mg mL^{-1}) of BCN-BSA/PNIPAM-co-MAA nanoconjugates, and 30 μL of a solution (40 mg mL^{-1}) of NHS-PEG35 in Na_2CO_3 buffer (pH 8.5, 100 mM) were gently mixed together. 1 mL of 2-ethyl-1-hexanol was gently added on top of the water phase, and the biphasic solution shaken manually for 10 s to produce a white turbid solution. The same procedure was employed to prepare the azide-functionalized proteinosomes in oil except that N_3-BSA/PNIPAM-co-MAA nanoconjugates were employed as the membrane building block.

Gently shaken oil suspensions of the azide- and alkyne-functionalized proteinosomes were mixed at a 1 : 1 ratio, and left to crosslink and co-sediment to the bottom of the vial for at least 2 h. Subsequently, the oil phase was carefully removed and replaced with 1 mL of Na_2CO_3 buffer (pH 8.5, 100 mM) containing 10 μL of a 8 mg mL^{-1} aqueous solution of a non-bio-orthogonal BSA/PNIPAM-co-MAA nanoconjugate. The vial was manually shaken for 10 s to produce a white w/o/w emulsion that migrated towards the meniscus. The water phase was carefully removed and replaced with 100 μL of a 40 mg mL^{-1} solution of NHS-PEG16-DS in water, and the vial was let to stand at room temperature and in the dark for 72 h. The oil layer was then removed by dialysis against water/70 % ethanol for 3-4 h, followed by against water/30 % ethanol for 3-4 h, and then 100 % water for 18 h to produce membrane-bounded prototissue spheroids.

To generate uncaged bio-orthogonally ligated proteinosome spheroids, 100 uL of a 0.5 M solution of sodium azide were added per mL of prototissue solution, and the outer proteinosome membrane cleaved by treatment for 2 h in a solution 50 mM of TCEP (or GSH or DTT) and sodium azide at pH 8.5. The prototissues were then left to sediment overnight, and finally washed 3 times with clean water using gentle centrifugation.

3. Contractile behaviour of synthetic tissue-like spheroids

Caged or uncaged prototissue spheroids were introduced into a microscope channel slide (*ca.* 22 x 3 x 0.3 mm), which was placed on top of a heating plate installed on a fluorescence microscope mobile stage. The temperature was regulated through a thermostat, and allowed to equilibrate for at least 5 min before acquiring the images. The sample temperature was verified through the use of an IR camera (FLIR E5). Changes in the prototissue volume were determined using ImageJ software. Measurements were repeated three times on different prototissue spheroids. Similar experiments were undertaken on caged or uncaged prototissue spheroids containing different numbers of bio-orthogonally linked proteinosomes, as well as on samples of individual proteinosomes.

To increase the rate of pulsation, a nichrome wire was connected to a DC power generator (model 71-10480, 0-30V, 3A; Tenma) and placed inside a microscope channel slide along with a sample of the caged or uncaged prototissue spheroids. Subsequently, a K-type thermocouple (EL-USB-2-LCD; Lascar Electronics) was also introduced into the microscope channel slide to monitor the solution temperature *in situ* and in real time. A contraction was stimulated by supplying current through the nichrome wire (1.500 A, 5.60 V) until the solution temperature reached 45 ^{o}C, at which point the DC power generator was switched off. Relaxation of the prototissue spheroid was then achieved by rapidly dissipating the heat using a water/ice/NaCl bath, which was placed on top of the microscope slide. The heating/cooling cycle was repeated at least 10 times. Images were captured on video using the fluorescence microscope.

4. Enzyme cascade reactions within prototissue spheroids

Room temperature studies (glucose/Amplex Red): Water-in-oil dispersions of cross-linked GOx-containing FITC-labelled BCN-BSA/PNIPAM-co-MAA proteinosomes or crosslinked HRP-containing unlabelled N_3-BSA/PNIPAM-co-MAA proteinosomes were prepared separately using the above procedures except that aqueous solutions of GOx (12 μL; 1 mg mL^{-1}) or HRP (6 μL; 1 mg mL^{-1}) were mixed with a solution of the BCN-BSA/PNIPAM-co-MAA or N_3-BSA/PNIPAM-co-MAA nanoconjugates, respectively. The enzyme-containing Pickering emulsions were mixed at a 1: 1 ratio and uncaged prototissue spheroids prepared as described above. Residual enzymes in the surrounding aqueous solution arising from proteinosome fragmentation during sample preparation were removed by gentle centrifugation

To monitor the onset and development of the GOx/HRP enzyme cascade within the synthetic prototissue spheroids incubated at 25 ^{o}C, a freshly prepared solution of Amplex Red (10 μL; 2.5 mM) was mounted on a PEGylated glass coverslip, and 40 μL of an aqueous dispersion of the uncaged GOx/HRP-containing prototissue spheroids was then added. The location of the GOx-containing FITC-labelled BCN-BSA/PNIPAM-co-MAA proteinosomes within individual prototissue spheroids was then imaged by fluorescence microscopy (time, t_0). Subsequently, a freshly prepared glucose solution (2.5 μL, 300 mM) was carefully added to the Amplex Red/prototissue dispersion (final glucose and Amplex concentrations; 14 mM and 0.5 mM, respectively), and the enzyme-mediated cascade synthesis of the fluorescent product resorufin was monitored spatially and analytically for 15 min using fluorescence confocal microscopy (λ_{exc} = 530 nm, λ_{em} = 600-670 nm).

Temperature-dependent studies (glucose/ABTS): Prototissue spheroids containing a 1:1 binary population of bio-orthogonally linked GOx-containing unlabelled BCN-BSA/PNIPAM-co-MAA proteinosomes and crosslinked HRP-containing unlabelled N_3-BSA/PNIPAM-co-MAA proteinosomes were prepared as above but with increased enzyme concentrations (GOx; 12 μL; 10 mg mL^{-1}) or HRP (5 μL; 10 mg mL^{-1}). Typically, an aqueous solution of freshly prepared 2,2'-azino-bis(3-ethylbenzothiazoline-6-sulphonic acid) (ABTS; 30 μL, 0.6 mM), followed by an aqueous solution of glucose (30 μL, 30 mM) was added to 120 μL of an aqueous dispersion of the GOx/HRP-containing uncaged prototissue spheroids to initiate the enzyme cascade reaction. Production of the oxidized green product ($[ABTS]^{\bullet+}$) was monitored at range of temperatures between 25 and 45°C by UV-Vis spectroscopy using a plate reader (BMG LABTECH CLARIOstar High Performance Monochromator Multimode Microplate Reader). Data points were acquired every 0.5 s over a duration of 180 s. The initial enzyme reaction rate was calculated using the following equation:

$$v_0 = \frac{\Delta A}{\Delta t \cdot \varepsilon \cdot b([E_1]+[E_2])} \qquad (1)$$

where, $\Delta A/\Delta t$ was the initial change of absorbance with time, ε the extinction coefficient of $[ABTS]^{\bullet+}$ (ε_{420} = $3.6 \cdot 10^4$ M^{-1} cm^{-1}), b the path length (1 cm, automatically corrected by the plate reader), and $[E_1]$ and $[E_2]$ the concentrations of the encapsulated GOx and HRP enzymes.

5. Contractile behaviour in hydrogelled prototissue spheroids

Water-in-oil dispersions of cross-linked GOx-containing FITC-labelled BCN-BSA/PNIPAM-co-MAA proteinosomes or crosslinked α-glucosidase (AGL)-containing RITC-labelled N_3-BSA/PNIPAM-co-MAA proteinosomes were prepared separately using the above procedures except that aqueous solutions of GOx (10 μL; 10 mg mL^{-1}) or AGL (20 μL; 10 mg mL^{-1}) were mixed with a solution of the BCN-BSA/PNIPAM-co-MAA or N_3-BSA/PNIPAM-co-MAA nanoconjugates, respectively. The enzyme-containing Pickering emulsions were mixed at a 1 : 1 ratio and uncaged prototissue spheroids prepared as described above. Residual enzymes in the surrounding aqueous solution were removed by gentle centrifugation.

To initiate the AGL/GOx-mediated hydrogelation of the prototissue spheroids, an aqueous dispersion of the 1 : 1 proteinosome mixture (17 μL) in an Eppendorf tube was diluted with a freshly prepared aqueous solution of Fmoc-Ala-Ala-OH (14.8 μL; 67.6 mM, pH 8.5) and Hoechst 33258 dye (1 μL, 1 mM), followed by addition of maltose (67.2 μL, 1.5 M) (Fmoc-Ala-Ala-OH, maltose and Hoechst 33258 final concentrations; 10 mM, 1 M and 0.01 mM, respectively). The dispersion was transferred into a microscope channel slide, which was then sealed. Hydrogelation of the prototissue over a period of 6-8 h at 25 °C was monitored spatially and analytically using fluorescence microscopy to determine the increase in blue fluorescence associated with sequestration of Hoechst 33258 within the growing dipeptide nanofilaments of the developing hydrogel. The corresponding decrease in pH associated with AGL/GOx-mediated gluconic acid production was monitored in control experiments undertaken over 24 h in the absence of Fmoc-Ala-Ala-OH. Data points were acquired automatically every 10 sec.

To study the contractile behaviour of the hydrogelled tissue-like spheroids, individual prototissues were subjected to 6 h of the AGL/GOx reaction, and then placed on top of a heating plate installed on a fluorescence microscope mobile

stage. The temperature was regulated through a thermostat, and allowed to equilibrate for at least 5 min before acquiring images of the prototissue at different temperatures. The sample temperature was verified through the use of an IR camera (FLIR E5). To restore maximum amplitude and reversible contractibility, the irreversibly contracted hydrogelated spheroids were introduced into an Eppendorf tube and centrifuged (1 min at 0.8 rpm, followed by 1 min at 2000 rpm). The supernatant was then removed and replaced with Na_2CO_3 buffer (0.1 M, pH 8.5).

Differential scanning calorimetry (DSC) measurements were performed on bulk peptide hydrogels using a TA Instruments DSC100 instrument. The hydrogel was prepared by adding to a 1.75 mL glass vial a freshly prepared solution of Fmoc-Ala-Ala-OH in water (148 μL; 67.6 mM, pH 8.5), a freshly prepared solution of AGL/GOx in water (180 μL; GOx 5 μL, 10 mg mL^{-1}; AGL 10 μL, 10 mg mL^{-1}), and a freshly prepared solution of maltose in water (672 μL, 1.5 M). The vial was incubated at room temperature for 18 h.

6. Characterization

Matrix-assisted laser desorption/ionization time of flight mass spectrometry (MALDI-TOF MS) was performed on a 4700 Proteomics analyzer (Applied Biosystems). The preparation of protein, protein/PNIPAM-co-MAA and PNIPAM-co-MAA samples required three solutions; (i) 3 equivalents of DHAP in EtOH (20.3 mg mL^{-1}) and 1 equivalent DAHC in water (18 mg mL^{-1}), (ii) 2 vol % TFA in water, and (iii) 1-5 mg $mL^{-1}$of protein, polymer or protein-polymer nanoconjugate in water. The three solutions were mixed in 1:1:1 ratio and spotted on the MALDI plate. Alternatively, polymer samples were prepared by mixing a *trans*-2-[3-(4-*tert*-butylphenyl)-2-methyl-2-propenylidene]malononitrile matrix (20 mg mL^{-1} in THF) with the polymer sample (2-8 mg·mL^{-1} in THF) at a 10:1 (v/v) ratio.

GPC characterization of PNIPAM-co-MAA was carried out using a Viscotek GPCmax equipped with a UV-Vis detector operating at 240 nm, differential refractometer and a column oven (35 °C). A flow rate of 1.0 mL min^{-1} in $n$$Bu_4NBr$/THF (0.1 % wt. $n$$Bu_4NBr$) was used and the column was calibrated with polystyrene standards.

^1H and ^{13}C spectra were recorded on a Varian 400 MHz spectrometer. ^1H NMR spectra are reported as δ in units of parts per million (ppm) relative to chloroform (δ 7.26, s). The number of protons (*n*) for a given resonance is indicated as *n*H, and was based on spectral integration values. ^{13}C NMR spectra are reported as δ in units of parts per million (ppm) relative to $CDCl_3$ (δ 77.23, t).

FTIR spectra were recorded using a Perkins Elmer Spectrum One spectrophotometer equipped with an ATR sampling accessory. Polymer and protein/polymer nanoconjugate samples were measured directly as solids, and the blank was automatically subtracted from each spectrum.

Circular dichroism (CD) spectroscopy was performed on a Jasco J-810/5 spectrometer. Spectra were recorded from 260 to 190 nm at 50 nm min^{-1} with at least 8 accumulations. Aqueous samples of N_3-BSA/PNIPAM-co-MAA and BCN-BSA/PNIPAM-co-MAA (0.2 mg mL^{-1}) were run in a 0.1 cm quartz cuvette cell.

DLS and zeta-potential measurements were performed on a ZETASIZER Nano series instrument (Malvern Instruments, UK) using 1 mg/mL solutions.

Optical and fluorescence microscopy was performed on a Leica DMI3000 B manual inverted fluorescence microscope at 20x and 63x magnification. A heating plate was installed to perform the temperature-dependent measurements on proteinosomes and 3D tissue-like spheroids. Images were analyzed using ImageJ software.

Confocal microscopy images were obtained on a Leica SP8 AOBS confocal laser scanning microscope attached to a Leica DM I6000 inverted epifluorescence microscope with 'Adaptive Focus Control' to correct focus drift during time-courses. The microscope was equipped with the following lasers; 65 mW Ar (458, 476, 488, 496, 514 nm lines), 20 mW solid state yellow (561 nm), 2mW Orange HeNe (594 nm), 10 mW Red He/Ne (633 nm) and a 50 mW 405 nm diode. All measurements were performed in an environmental chamber maintained at 25 ºC. Images were analyzed using ImageJ software.

7. Preparation of polymers, derivatized proteins, and bio-orthogonal protein/polymer nanoconjugates

PNIPAM-co-MAA: *N*-isopropylacrylamide and AIBN were freshly recrystallized from hexane and methanol, respectively. *N*-isopropylacrylamide (0.900 g; 7.95 mmol), methacrylic acid (50 mg, 0.58 mmol; 6.8 mol/mol %, 5 wt %), AIBN (2.4 mg, 15 μmol), and mercaptothiazoline-activated RAFT agent (25 mg, 68 μmol)[23] were dissolved in 4 mL of acetonitrile in a small round bottom flask equipped with a stirrer bar. The solution was purged with argon for 30 min and the flask sealed. Polymerization was carried out at 65 ºC for 8 h with stirring at 700 rpm. The polymer was isolated by precipitation from 1:1 hexane/Et_2O (250 mL) as a crystalline light-yellow powder in 96 wt % yield. M_n 13,000 g mol^{-1}, PDI 1.06 (GPC), 5 wt % in methacrylic acid.

Labelling of BSA with fluorescent dyes: In general, 20.9 mg of BSA were dissolved in 7.74 mL of Na_2CO_3 buffer (pH 8.5, 100 mM), and 193.5 μL of a DMSO solution of a fluorescent dye (1.0 mg mL^{-1}, FITC, RITC, or DyLight405-NHS) added. The conjugation reaction was performed for 5 h at room temperature. The fluorescent dye-conjugated BSA was purified by dialysis, lyophilized and stored as a solid at -20 ºC.

Cationization of BSA: In a vial, 18 mg of non-fluorescent or fluorescent dye-labelled BSA were dissolved in 1.8 mL of water. In a separate vial, 180 mg of hexamethylenediamine were dissolved in 1.8 mL of water and the pH was adjusted to 6.0. The hexamethylenediamine solution was slowly added to the BSA solution under vigorous stirring, and the pH readjusted to 6.0. The cationization reaction was initiated by adding 9.0 mg of EDAC dissolved in 500 μL of water. After 2 h, another 9 mg of EDAC dissolved in 500 μL of water were added. The reaction was left under stirring at room temperature for 18 h. BSA-NH_2 was purified by dialysis, centrifuged (5 min, 5000 rpm) to remove any precipitate, and then lyophilised and stored as a solid at -20 ºC. On average, this procedure resulted in a 30 % level of cationization as determined by MALDI-TOF spectrometry.

BSA/PNIPAM-co-MAA: In a vial, 20 mg of cationized BSA were dissolved in 10 mL of Na_2CO_3 buffer (pH 8.5, 100 mM). In a separate vial, 20 mg of mercaptothiazoline-activated PNIPAM-co-MAA were dissolved in 10 mL of water. The mercaptothiazoline-activated PNIPAM-co-MAA solution was added dropwise to a stirred solution of cationized BSA, and the conjugation reaction carried out for 18 h at room temperature. BSA-NH_2/PNIPAM-co-MAA was then isolated by centrifugation using centrifugal filters with 50,000 Da MWCO. The residues were washed 4 times to remove any unreacted polymer, and the product lyophilised and stored as a solid at -20 ºC.

Bio-orthogonal BSA/PNIPAM-co-MAA nanoconjugates: In a vial, 10 mg of BSA/PNIPAM-co-MAA were dissolved in 9.8 mL of water. In a separate vial, 10 mg of BCN-NH_2 (3.1 μmol) or N_3-NH_2 (4.6 μmol) were dissolved in 100 μL of DMSO. The BCN-NH_2 or N_3-NH_2 solution was slowly added to the stirred BSA/PNIPAM-co-MAA solution, and the pH adjusted to 6.0. The coupling reaction was initiated by the addition of 5 mg of EDAC (2.6 μmol) dissolved in 100 μL of water. After 1 h the pH was raised to 8.0, and the reaction carried out at room temperature for 18 h. The bio-orthogonal BSA nanoconjugates were purified by dialysis, centrifuged to remove any precipitate, and then lyophilised and stored as a solid at -20 ºC.

8. Permeability studies for caged and uncaged prototissue spheroids

Experiments were performed by mixing 40 μL of solutions 0.1 mg/mL of FITC-labelled dextran (FITC-Dextran, Sigma-Aldrich) with a molecular weight ranging from 4 to 150 kDa, with 40 μL of a prototissue spheroid or proteinosome aqueous dispersion. The polymer solution and the prototissue or proteinosome dispersion were pre-equilibrated either at 25 or 47 ^{o}C before mixing. All data were based on normalized fluorescence intensity value determined from fluorescence microscopy images using ImageJ software.

9. Prototissue force measurements using atomic force microscopy (AFM)

The external force induced by the thermoresponsive expansion of individual prototissue spheroids was investigated by AFM. A Multi-mode VIII microscope with Nanoscope V (Bruker, CA, USA) controller was utilized in combination with a fluid cell and Bio-Heater mount. For bulk measurements of the expansion-induced radial force, a micro-cantilever was used with a spring constant of 0.055 N/m, as calibrated via thermal tuning. A silica microsphere of radius 7 μm was attached to the cantilever to produce a colloidal cantilever, and thereby ensure a large contact area between the cantilever and prototissue spheroid and reduce the risk of "puncturing" the expanding surface. A dispersion of the prototissues (40 μL) was deposited on freshly cleaved mica before being sealed in the fluid cell. An individual prototissue spheroid was identified optically, heated to 50°C and allowed to equilibrate before being trapped between the mica and the microsphere of the colloidal cantilever. The deflection of the cantilever was monitored in real time as the prototissue cooled to 30°C. The radial force induced by expansion of the spheroid was calculated by the application of Hooke's law ($F(x) = kx$, where x is the deflection of the cantilever and k is the cantilever spring constant). Measurements were repeated for three heating-cooling cycles on an individual prototissue spheroids. Background contributions associated with the deflection measurements were deconvoluted by undertaking force measurements directly at the surface of the mica substrate (control experiments).

Acknowledgements
We thank NSERC Canada (PDF-487171-2016) and EU Horizon 2020 (Marie Skłodowska-Curie grant No. 701876) for funding, and the NMR/Mass Spectrometry Facility, the Wolfson Bioimaging Facility (Dr A. Leard; BBSRC grant BB/L014181/1), and Chemical Imaging Facility (EPSRC grant *"Atoms to Applications"* EP/K035746/1) for help with physical characterization. We thank Prof. I. Manners, J. Finnegan and S. Briggs for assistance with GPC/DSC measurements, Prof D. Woolfson for use of dichroism (CD) and plate reader spectrometers (BBSRC/EPSRC Bristol Synthetic Biology Research Centre (BB/L01386X/1)), Dajana Gubala for help with AFM measurements, Dr N. Martin and Dr R. Booth for fruitful discussions, Dr T. Ferrugia for assistance with the development of a customized microscope heating stage, and Prof T. Liverpool for mathematical discussions.

Author contributions
PG, AJP, ML and SM conceived the experiments; PG performed the experiments; PG and RH performed the force measurements; WB and PG developed the theoretical model for the prototissue expansion force. All authors undertook data analysis, discussed the results, and contributed to drafts of the manuscript; PG and SM wrote the final manuscript.

Additional information
Supplementary information is available in the online version of the paper. Reprints and permissions information is available online at … . Correspondence and requests for materials should be addressed to S.M.

Competing financial interests
The authors declare no competing financial interests.

Data availability statement
The authors declare that all relevant data supporting the finding of this study are available within the paper and its Supplementary Information files. Additional data are available from the corresponding author upon request.

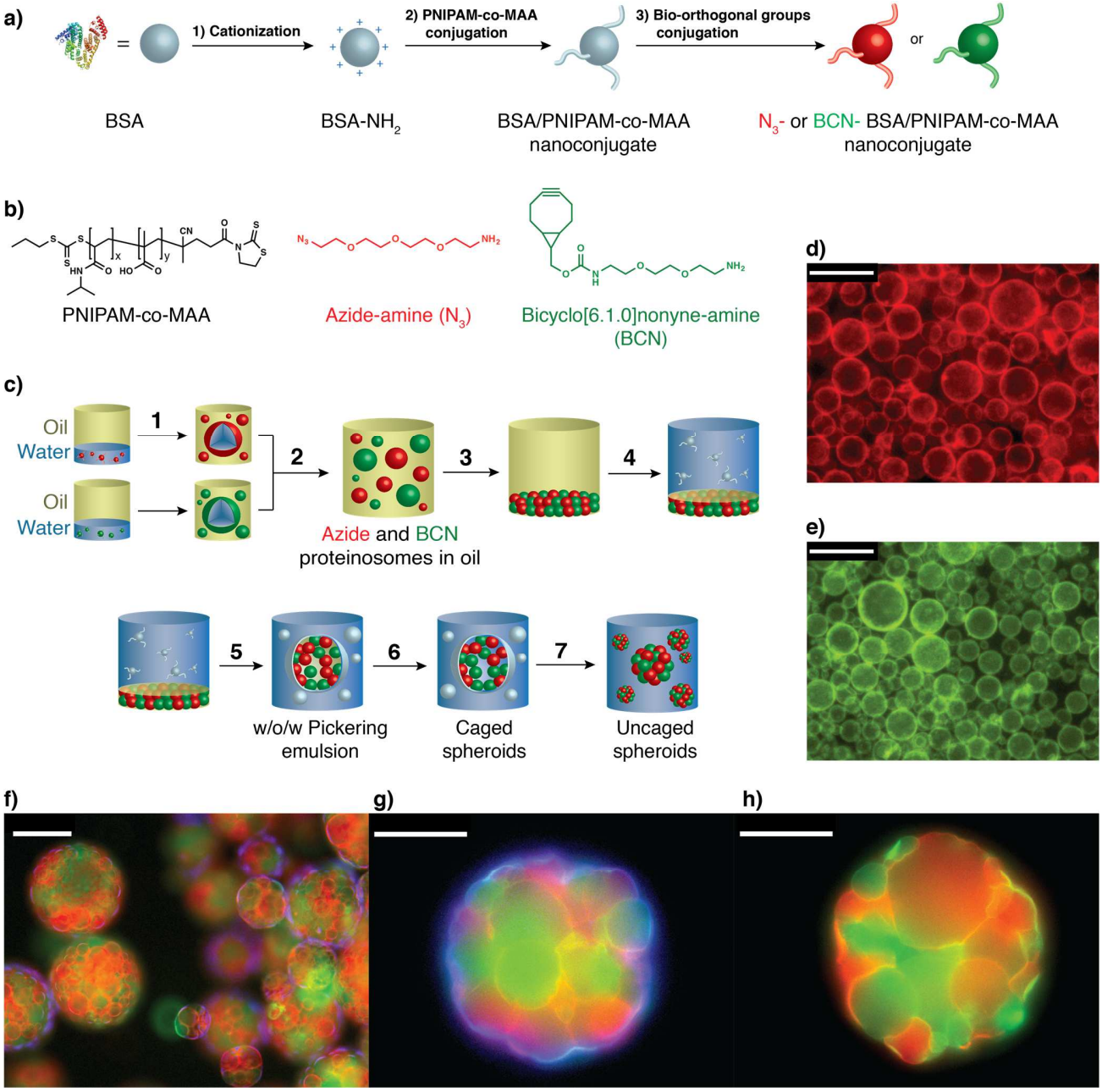

Figure 1: Programmed assembly of proteinosomes into synthetic prototissue spheroids. a, Synthesis pathway for the preparation of amphiphilic thermoresponsive protein-polymer nanoconjugates with bio-orthogonal functionalities. **b**, Molecular structures of the activated co-polymer (PNIPAM-co-MAA) and bio-orthogonal prosthetic groups (azide-amine (N_3); bicyclo[6.1.0]nonyne-amine (BCN)). **c**, Scheme showing experimental procedure for the preparation of proteinosome-based prototissue spheroids. **d,e**, Fluorescence optical microscopy images showing single populations of rhodamine isothiocyanate (RITC)-labelled azide-functionalized proteinosomes (**d**) and fluorescein isothiocyanate (FITC)-labelled alkyne-functionalized proteinosomes (**e**) dispersed in oil; ; scale bars, 50 µm. **f-h**, Fluorescence optical microscopy images showing: **f**, w/o/w emulsion droplets consisting of caged multi-compartmentalized spheroids containing a closely packed mixture of RITC-labelled azide- (red) and FITC-tagged alkyne- (green) functionalized crosslinked proteinosomes dispersed in oil and incarcerated within a DyLight405-labelled non-bio-orthogonally crosslinked host proteinosome membrane (blue); **g**, individual membrane-bounded prototissue spheroid produced and dye-labelled as in (**f**), and consisting of a spatially interlinked network of closely packed bio-orthogonally ligated crosslinked proteinosomes (red and green) encased in and adhered to a non-bio-orthogonally crosslinked host proteinosome membrane (blue); **h**, uncaged spheroid after removal of

the outer proteinosome membrane with an intact bio-orthogonally interconnected tissue-like architecture. Scale bars in (**f**), (**g**), and (**h**) **=** 100, 50 and 50 µm, respectively. See Supplementary Notes, section 2.3 for figure legends with full details.

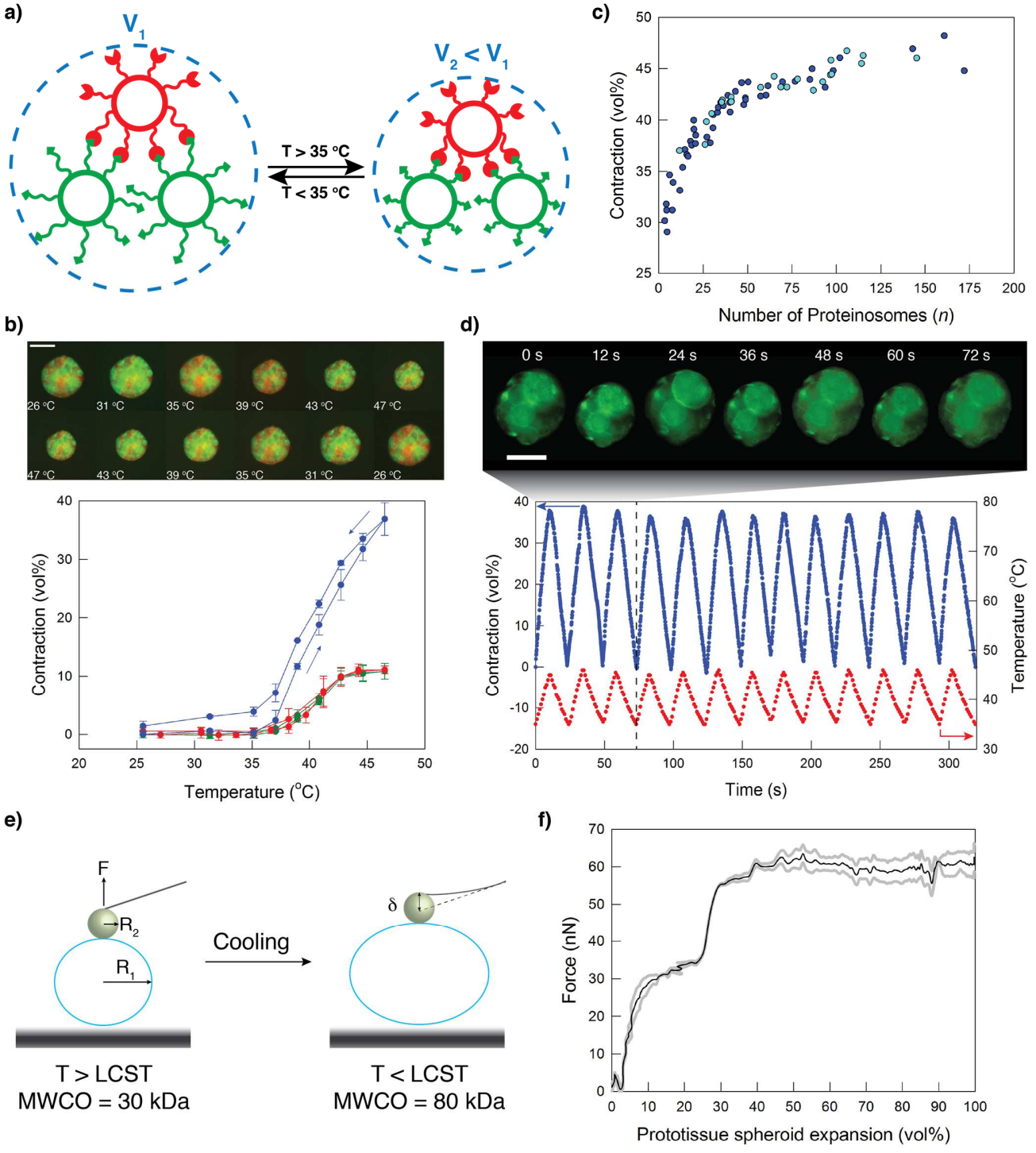

Figure 2: Collective contractile behaviour in prototissue spheroids. a, Scheme illustrating the temperature-dependent collective contractile behaviour of a prototissue spheroid (blue dashed circle) consisting of a binary population of bio-orthogonally ligated alkyne (green) and azide (red) functionalized proteinosomes; V_1 and V_2 are volumes associated with spheroids in the relaxed (T < 35 °C) or contracted (T > 35 °C) state, respectively. **b**, *Top image*: fluorescence microscopy images showing temperature-dependent reversible changes in the equilibrium volume of an individual uncaged prototissue spheroid; scale bar 50 µm. *Bottom image*: plots showing temperature-dependent reversible changes in the equilibrium volume of individual azide- (red) or alkyne- (green) functionalized proteinosomes, and single uncaged prototissue spheroids

(blue). **c**, Plot showing the temperature-dependent changes in the equilibrium volume of caged (azure) and uncaged (blue) prototissue spheroids as a function of the total number of constituent proteinosomes (*n*). **d**, *Top image*: snapshots of video images showing a single uncaged prototissue spheroid exhibiting three reversible oscillatory contractions/relaxations associated with repeated thermal cycling of the sample between 25 and 47 °C over a period of 72 s (dashed line in bottom image); scale bar, 50 µm. *Bottom image*: corresponding plot of spheroid volume against temperature showing direct correlation between the reversible contractibility and temperature ramps imposed on the system. A maximum contraction of *ca*. 37 vol% is observed during each temperature cycle. **e**,**f**, Prototissue force measurements using AFM. **e**, Schematic representation of the experiment design showing a contracted prototissue spheroid (blue circle) that is trapped at a temperature above the LCST between a mica surface and calibrated colloidal cantilever. Upon cooling below the LCST, the prototissue expands back to the native state and the cantilever deflection is quantified. The force exerted by the prototissue was calculated as the product of the cantilever deflection and cantilever spring constant (0.055 N/m) at different stages of expansion (Methods, section 9). **f**, Plot of force against volume% expansion for a single prototissue spheroid (grey lines represent standard deviation on 3 measurements). The first plateau in the force curve was attributed to reversible buckling of proteinosomes within the prototissue spheroid (see Supplementary Video 4). See Supplementary Notes, section 2.3 for figure legends with full details.

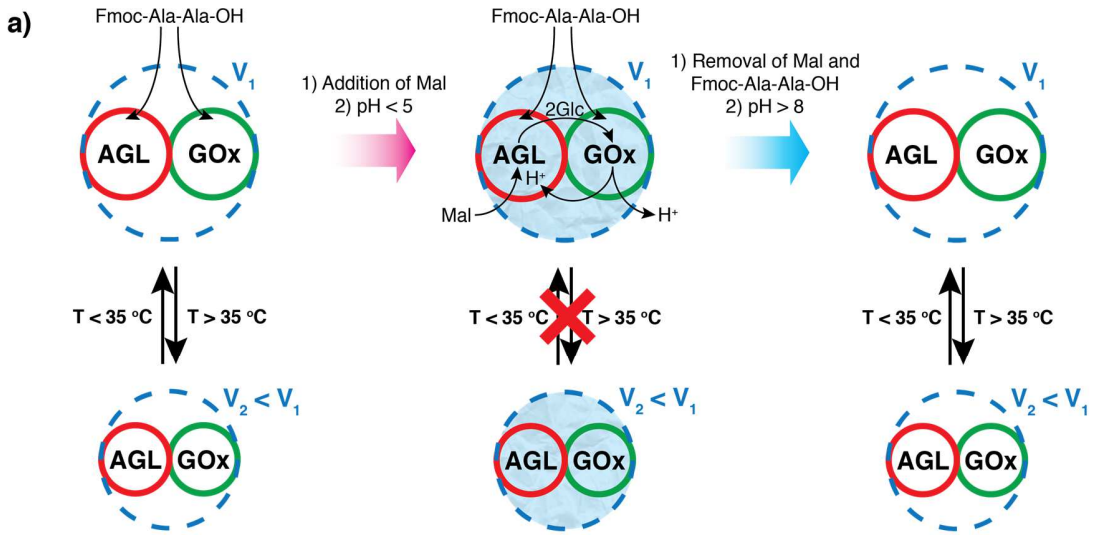
a)
Fmoc-Ala-Ala-OH
AGL
GOx
V1
1) Addition of Mal
2) pH < 5
2Glc
H+
Mal
1) Removal of Mal and
Fmoc-Ala-Ala-OH
2) pH > 8
T < 35 °C
T > 35 °C
V2 < V1

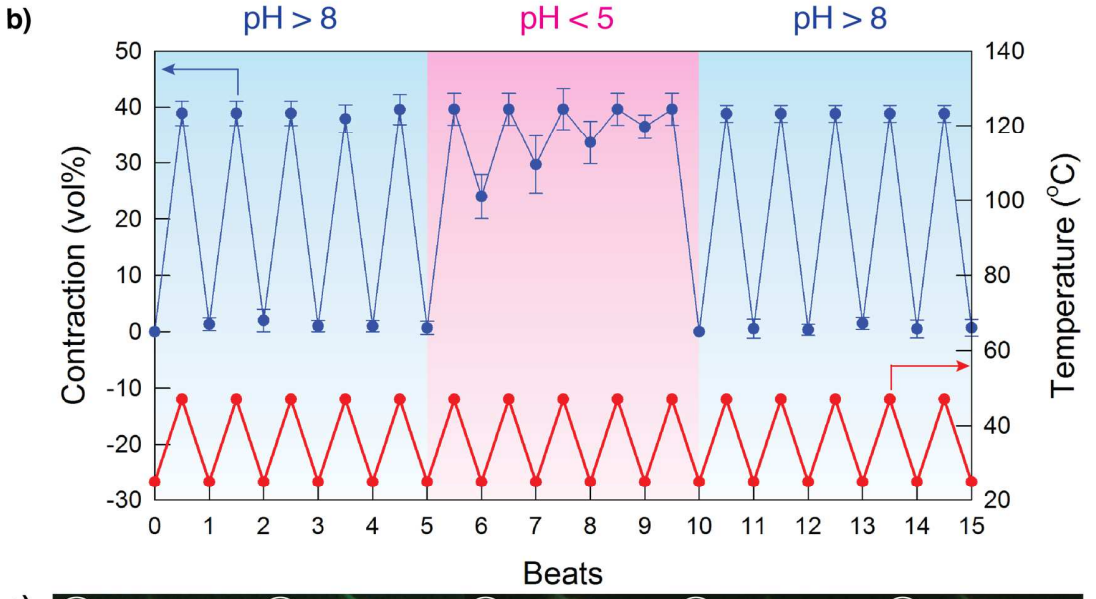
b)
pH > 8
pH < 5
pH > 8
Contraction (vol%)
Temperature (°C)
Beats

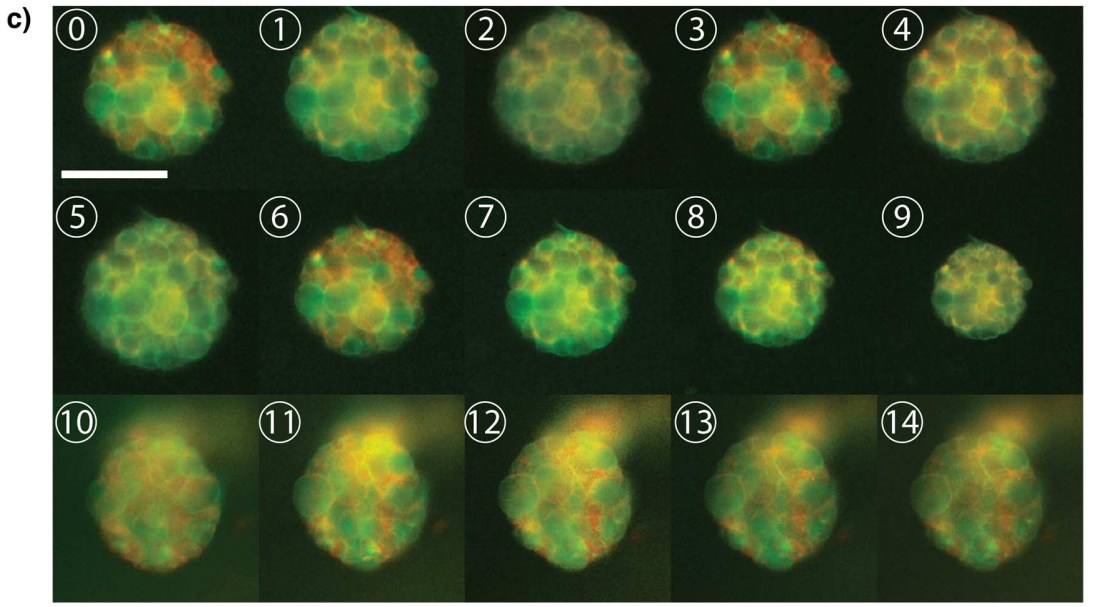
c)
0
1
2
3
4
5
6
7
8
9
10
11
12
13
14

Figure 3: Enzyme-mediated amplitude modulation within thermoresponsive prototissue spheroids. a, Scheme representing the coupling of contractile behaviour to a AGL/GOx cascade reaction within a prototissue spheroid (blue dashed circle) consisting of bio-orthogonally linked AGL-containing RITC-labelled azide-functionalized proteinosomes (red circles) and GOx-containing FITC-labelled alkyne-functionalized proteinosomes (green circles). The prototissue reversibly contracts/relaxes in the presence of peptide Fmoc-Ala-Ala-OH at pH 8.5 (*left*). Addition of maltose (Mal) triggers the enzyme cascade and reduces the pH below 5, initiating peptide hydrogelation, which hinders re-expansion (*centre*). Removal of Mal and Fmoc-Ala-Ala-OH, and restoration of an alkaline pH disassemble the hydrogel and re-establishes reversible contractile behaviour (*right*). **b**, Graph showing amplitude modulation of contractile behaviour of uncaged prototissue spheroids for conditions described in (**a**) for repeated thermal cycling between 25 and 47 °C (blue plot). Corresponding cycles in temperature are shown (red plot). **c**, Time-dependent fluorescence microscopy images acquired at 25 °C of a single prototissue spheroid subjected to the conditions described in (**a**) and (**b**) showing switching off and on of the reversible contractile behaviour. Red fluorescence, AGL-containing RITC-labelled azide-functionalized proteinosomes; green fluorescence, GOx-containing alkyne-functionalized proteinosomes. The beat number is indicated on the top-left of each image, and refers to the graph in (**b**), scale bar, 50 μm. See Supplementary Notes, section 2.3 for figure legends with full details.

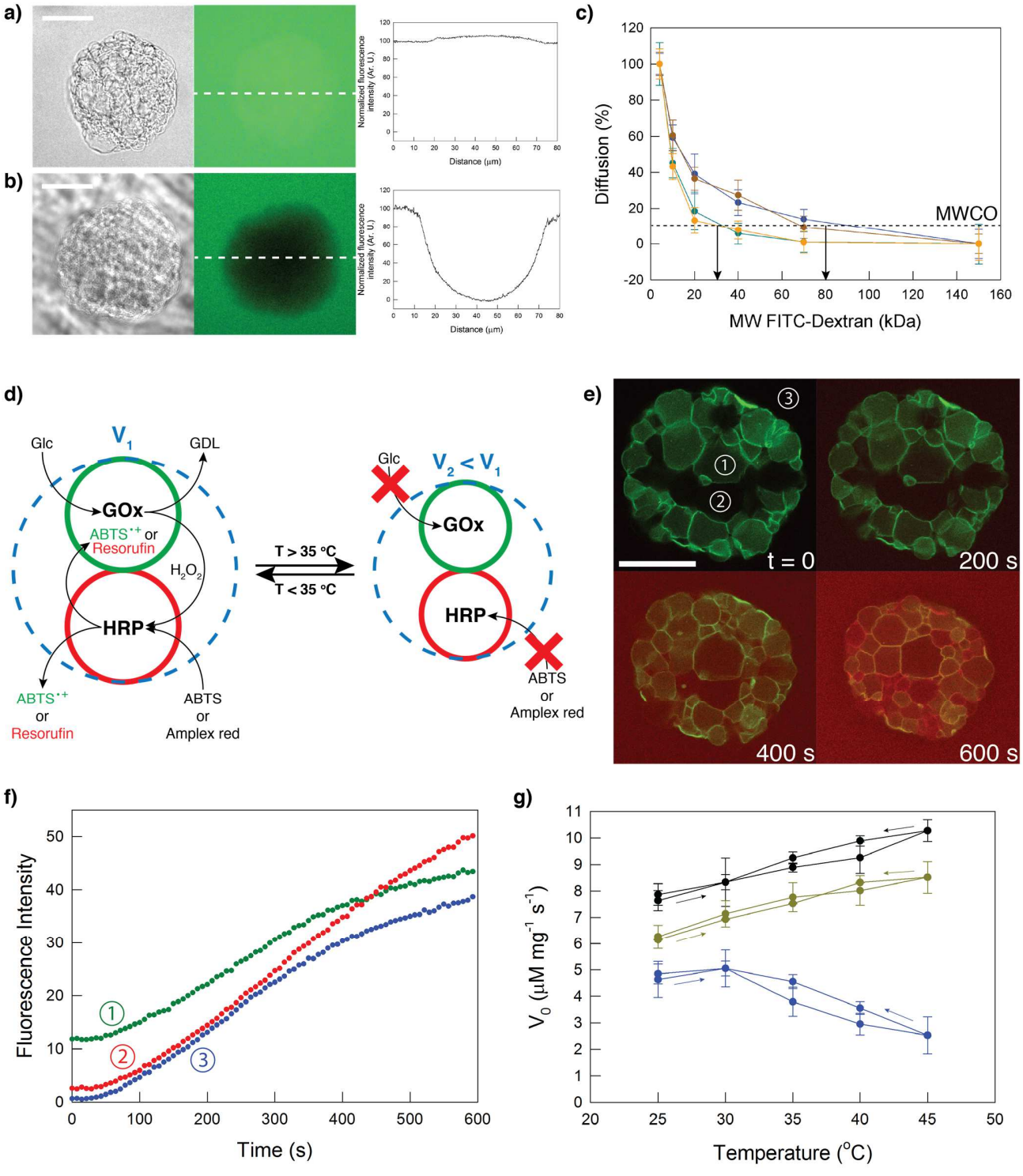

Figure 4: Mechanochemical transduction within prototissue spheroids. a,**b**, Optical (left) and fluorescence (middle) microscopy images and fluorescence intensity line profiles (right) recorded from individual caged proteinosomes after incubation at 25 ^{o}C in the presence of FITC-dextran with molecular weights of 4 (**a**) or 150 kDa (**b**) showing macromolecular uptake or exclusion, respectively. Dashed line in fluorescence microscopy images correspond to line intensity analysis; scale bars 25 μm. **c**, Plot of percentage diffusive uptake for caged and uncaged prototissue spheroids incubated in the presence of FITC-dextran of different molecular weights and at 25 (blue, caged; brown, uncaged) or 47 ^{o}C (dark cyan, caged; orange,

uncaged). Arrows indicate approximate MWCOs of 80 kDa at 25 °C and 30 kDa at 47 °C, corresponding to the relaxed and contracted states of the spheroids, respectively. **d**, Scheme representing coupling of the contractile behavior to a GOx/HRP enzyme cascade reaction in a prototissue spheroid (blue dashed circle) consisting of GOx-containing alkyne-functionalized proteinosomes (green circles) and HRP-containing azide-functionalized proteinosomes (red circles). In the relaxed prototissue (V_1), glucose (Glc) and ABTS or Amplex red freely diffuse through the system, and are transformed into D-Glucono-1,5-lactone (GDL) and green $ABTS^{\bullet+}$ or red fluorescent resorufin, respectively. In the contracted form (V_2), diffusion of the substrates towards the enzymes is hindered. **e**, Time-dependent confocal fluorescence microscopy images of a single uncaged prototissue spheroid prepared as described in (**a**) in the presence of glucose and Amplex Red at 25 °C. Green fluorescence, GOx-containing FITC-labelled alkyne-functionalized proteinosomes; red fluorescence, resorufin production; scale bar, 50 µm. Numbers shown at *t* = 0 s show selected areas used for fluorescence intensity measurements (see plot in **c**). **f**, Time-dependent plots of total fluorescence intensity recorded from selected regions of the spheroid shown in (**e**); (1) GOx-containing proteinosomes (green), (2) HRP-containing proteinosomes (red), and (3) external aqueous environment (blue). **g**, Plots of reversible temperature-dependent changes in initial reaction rates for GOx/HRP-mediated cascade reactions undertaken in the presence of glucose (5 mM) and ABTS (0.1 mM) for enzymes in free solution (control, black plot), a dispersed 1:1 population of non-coupled GOx-containing and HRP-containing proteinosomes (dark yellow plot), and GOx/HRP-containing prototissue spheroids (blue plot). See Supplementary Notes, section 2.3 for figure legends with full details.